Organic & Biomolecular Chemistry

RSC Publishing

PAPER

View Article Online
View Journal | View Issue

Cite this: *Org. Biomol. Chem.*, 2013, **11**, 7751

An OFF–ON chemosensor for biological and environmental applications: sensing Cd^{2+} in water using catanionic vesicles and in living cells†

Andrea Bencini,[a] Francesco Caddeo,[b] Claudia Caltagirone,*[b] Alessandra Garau,[b] Mike B. Hurstouse,[c,d] Francesco Isaia,[b] Sandrina Lampis,[b] Vito Lippolis,[b] Francesco Lopez,[e] Valeria Meli,[b] Maura Monduzzi,[b] Maria Cristina Mostallino,[f] Sergio Murgia,*[b] Stefano Puccioni,[a] Judith Schmidt,[g] Pietro Paolo Secci[f] and Yeshayahu Talmon[g]

A new OFF–ON fluorescent chemosensor (**L**^{1}) for Cd^{2+} recognition based on a 5-chloro-8-hydroxyquinoline pendant arm derivative of 1,4,7-triazacyclononane ([9]aneN$_3$) will be presented and its photochemical features in an MeCN–H_2O 1 : 1 (v/v) mixture, in pure water, after inclusion within catanionic vesicles, and in living cells will be discussed. The coordination properties of **L**^{1} both in solution and in the solid state were preliminarily studied and its selectivity towards Cd^{2+} *versus* a set of different metal ions (Cu^{2+}, Zn^{2+}, Cd^{2+}, Pb^{2+}, Al^{3+}, Hg^{2+}, Co^{2+}, Ni^{2+}, Mn^{2+}, Mg^{2+}, K^{+}, Ca^{2+}, Ag^{+}, and Na^{+}) was verified in MeCN–H_2O 1 : 1 (v/v). In water, upon addition of increasing amounts of Cd^{2+} to **L**^{1} an enhancement of the fluorescence emission was detected. To overcome this serious drawback, **L**^{1} was dissolved in an innovative catanionic vesicular solution based on sodium bis(2-ethylhexyl) sulfosuccinate, a traditional surfactant, and 1-dodecyl-3-methylimidazolium bromide, an ionic liquid. When enclosed within the vesicle bilayers in water, **L**^{1} restored its fluorescence emission property upon addition of Cd^{2+}. Remarkably, **L**^{1} enters the cellular membrane of living cells thus allowing the detection of intracellular Cd^{2+}. These findings encourage the application of this new fluorescent chemosensor in real samples for histological and environmental analyses.

Received 10th July 2013,
Accepted 16th September 2013

DOI: 10.1039/c3ob41420e

www.rsc.org/obc

Introduction

Among various heavy metal ions, cadmium(II) is one of the most dangerous due to its high toxicity and carcinogenicity.[1] It accumulates in the environment, contaminating food and water.[2] Smoking and inhalation of cadmium-containing dust represent additional sources of cadmium uptake in humans. Cadmium accumulation is involved in neurological, reproductive, cardiovascular, and developmental disorders.[3] Bearing in mind the elevated risks related to human health, assessment of cadmium accumulation both in the environment and in biological organisms can be considered to be an aspiration of primary importance. Common methods for the detection of heavy metal ions make use of atomic absorption spectrometry, inductively coupled plasma mass spectrometry, and anodic stripping voltammetry.[4–8] These analytical methods often require extensive sample preparation and high costs. Consequently, a simple and inexpensive method effective in the detection as well as quantification of heavy metal ions is desirable for real-time monitoring of environmental, biological, and industrial samples. Among the detection methods currently available, those based on optical and, in particular, fluorescence spectroscopy are the most convenient because of their simplicity and low detection limits.[9–13] It is also worth noting that one of the most important advantages of a fluorescent probe would be intracellular detection although, to the best of our knowledge,

[a]*Dipartimento di Chimica "Ugo Schiff", Università degli Studi di Firenze, Via della Lastruccia 3, 50019 Sesto Fiorentino, FI, Italy*
[b]*Dipartimento di Scienze Chimiche e Geologiche, Università degli Studi di Cagliari, S.S. 554 bivio per Sestu, I-09042 Monserrato, CA, Italy. E-mail: ccaltagirone@unica.it, murgias@unica.it*
[c]*School of Chemistry, University of Southampton, Southampton, UK*
[d]*Department of Chemistry, Faculty of Science, King Abdulaziz University, Jeddah 21588, Saudi Arabia*
[e]*Dipartimento di Agricoltura, Ambiente Alimenti (DIAAA) and Consorzio Interuniversitario per lo Sviluppo dei Sistemi a Grande Interfase (CSGI), Università degli studi del Molise, I-86100 Campobasso, Italy*
[f]*Istituto di Neuroscienze (CNR), Cagliari, S.S. 554 bivio per Sestu, I-09042 Monserrato, CA, Italy*
[g]*Department of Chemical Engineering, Technion – Israel Institute of Technology, Haifa 32000, Israel*

†Electronic supplementary information (ESI) available: Experimental methods and materials, synthesis of **L**^{1} and of $[Cu_4(\mathbf{L}^{1})_2](ClO_4)_2$, absorption and emission spectra of **L**^{1} with all the metal ions, SAXS spectra, crystallographic tables, effect of the Cd^{2+} concentration on cells fluorescence. CCDC 949184. For ESI and crystallographic data in CIF or other electronic format see DOI: 10.1039/c3ob41420e

few examples of Cd^{2+} detection in living cells have been reported to date.[14–17]

Recently, different highly selective and sensitive chemical sensing systems for the chromogenic and fluorogenic recognition of Cd^{2+} have been developed by immobilizing Cd^{2+}-selective chromophores or receptors into different materials such as QD (quantum dots),[18] silver nanoparticles,[19] cubic *Fm3m* cage monolites,[20,21] graphene sheets,[22] and so on with the aim of increasing the performances of the chromophores/receptors. Although previously cited examples of nanomaterials used to support Cd^{2+}-selective chemosensors all belong to the hard matter, also their soft matter counterparts may be taken into account as suitable candidates for the same goal. Indeed, self-assembled materials such as vesicles[23–26] or polymeric nanoparticles[27–31] were, a long time ago, proposed to be useful nanocarriers for hydrophobic molecules. Thus, they can properly be used to simultaneously solubilize in water highly hydrophobic fluorescence chemosensors and protect them from solvent quenching while leaving unaltered or, possibly, increasing their detection ability.

In the following, we will show how such an aim can be pursued entrapping into the bilayer of innovative catanionic vesicles a newly synthesized OFF–ON chemosensor ($\mathbf{L^1}$) for Cd^{2+} recognition based on the macrocycle 1,4,7-triazacyclononane as the receptor unit and three moieties of 5-chloro-8-hydroxyquinoline as the fluorogenic unit. Catanionic vesicles were chosen since they offer several advantages over conventional phospholipid based liposomes. Actually, catanionic vesicles form spontaneously, without energy input, upon a simple mixing of two separate surfactant solutions; in many cases they exist as equilibrium self-assembled structures (therefore they are indefinitely stable), they allow for surface charge regulation (basically varying the surfactant mixing ratio), and they typically show an extremely low (in the range of μM) critical aggregation concentration.[32–35] Here, this kind of colloidal suspension was obtained by mixing sodium bis(2-ethylhexyl) sulfosuccinate (NaAOT), a traditional vesicle forming anionic surfactant, and 1-dodecyl-3-methylimidazolium bromide (C_{12}mimBr), an ionic liquid based cationic surfactant. Ionic liquids, in particular, represent a class of electrolytic solvents composed of large and asymmetric organic cations and small inorganic anions that have been shown to possess peculiar properties in water and that can also be used for the preparation of innovative formulations.[36,37]

In this paper the physicochemical and morphologic characteristics of the catanionic vesicles and the photochemical features of $\mathbf{L^1}$ in both MeCN–H_2O 1 : 1 (v/v) mixture and in pure water after the entrapment into the catanionic vesicle bilayers will be reported and discussed. In addition, the possibility that $\mathbf{L^1}$ can be effective in Cd^{2+} detection in living cells will be demonstrated.

Results and discussion

Synthesis and coordination chemistry of $\mathbf{L^1}$

$\mathbf{L^1}$ was synthesised *via* a Mannich reaction as shown in Scheme 1. The macrocycle 1,4,7-triazacyclononane[38] reacted with 3 equivalents of 5-chloro-8-hydroxyquinoline in the presence of paraformaldehyde in toluene at 90 °C under a nitrogen atmosphere to give the desired ligand in 62% yield (see ESI† for details). The protonation behaviour of $\mathbf{L^1}$ was studied by means of potentiometric measurements at 298.1 K, using MeCN–H_2O (1 : 1 v/v) as a solvent because of the low solubility of the ligand in pure H_2O. Ligand $\mathbf{L^1}$ binds just a single proton at acidic pH values (Table 1 and Fig. 1) to give the $(H\mathbf{L^1})^+$ species.

Conversely, in the alkaline pH region (Table 1 and Fig. 1), $\mathbf{L^1}$ undergoes two successive deprotonation equilibria, to form the $(\mathbf{L^1}(H_{-1}))^-$ and $(\mathbf{L^1}(H_{-1})_2)^{2-}$ anionic species. These data account for the formation in solution of species containing one or two deprotonated 5-chloro-8-hydroxyquinoline units. On the other hand, polyamines with aromatic or heteroaromatic –OH groups adjacent to amine functions can also be in zwitterionic form.[39] Therefore, the observed deprotonation steps of $\mathbf{L^1}$ could imply either acidic dissociation of the hydroxyl units of the 5-chloro-8-hydroxyquinoline moieties or, supposing $\mathbf{L^1}$ in a zwitterionic form, deprotonation of the ammonium groups of the [9]aneN_3 unit.

Clearly, the potentiometric measurements and their treatment using the program HYPERQUAD[40] do not allow one to

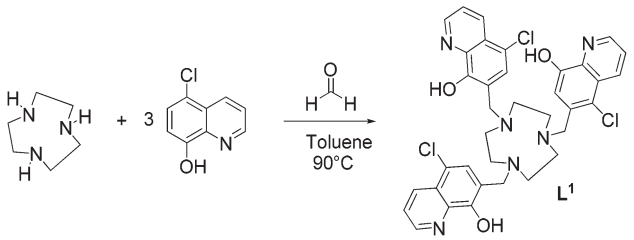

Scheme 1 Synthesis of $\mathbf{L^1}$.

Table 1 Constants (log units) for the protonation and deprotonation equilibria of $\mathbf{L^1}$ in MeCN–H_2O (1 : 1 (v/v) at 298.1 K), 0.10 M NMe_4Cl

$\mathbf{L^1} + H^+ = (H\mathbf{L^1})^+$	$pK_a = 2.67(4)$
$\mathbf{L^1} = (\mathbf{L^1}(H_{-1}))^- + H^+$	$pK_a = 8.24(5)$
$(\mathbf{L^1}(H_{-1}))^- = (\mathbf{L^1}(H_{-1})_2)^{2-} + H^+$	$pK_a = 9.80(1)$

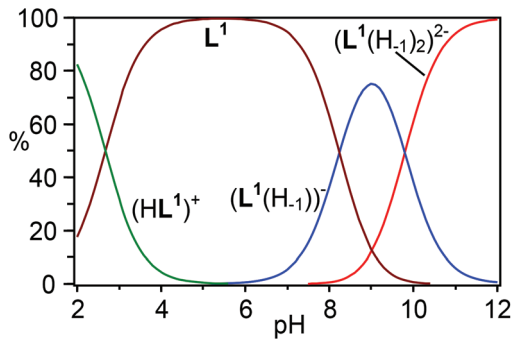

Fig. 1 Distribution diagram of the protonated/deprotonated species of $\mathbf{L^1}$ (MeCN–H_2O, 1 : 1 v/v, 298.1 K, 0.10 M NMe_4Cl, $[\mathbf{L^1}] = 1.0 \times 10^{-3}$ M).

distinguish the protonation/deprotonation sites within the ligand structure, but only to determine the corresponding equilibrium constants. On the other hand, the measured pK_a values are in the range normally found for protonation of polyamines and only somewhat lower than the pK_a value of 5-chloro-8-hydroxyquinoline (pK_a = 10.64 in a water–dioxane 60 : 40 v/v mixture).[41]

However, ^{1}H-NMR spectra recorded at different pH values show that deprotonation of $\mathbf{L^1}$ to give $(\mathbf{L^1}(H_{-1}))^-$ and $(\mathbf{L^1}(H_{-1})_2)^{2-}$ is accompanied by a marked upfield shift of the signals of the methylene groups HA and HB (see Fig. 2), in α-position to the aliphatic amine groups of the macrocyclic moiety, as normally observed in the case of deprotonation of ammonium groups. This suggests that the formation of the $(\mathbf{L^1}(H_{-1}))^-$ and $(\mathbf{L^1}(H_{-1})_2)^{2-}$ species of the ligand is accompanied by deprotonation of the ammonium groups, *e.g.*, ligand $\mathbf{L^1}$ is in zwitterionic form with at least two protonated amines and two deprotonated hydroxyl functions. However, Fig. 2 also shows that the signals of the 5-chloro-8-hydroxyquinoline moieties are also affected by ligand deprotonation, even if to a lower extent than the HA and HB resonances. This may indicate that in $\mathbf{L^1}$ the acidic protons are partially localized (and/or shared *via* hydrogen bonding) on the deprotonated hydroxyl groups. A similar proton distribution has already been observed in other [9]aneN$_3$ macrocycles with appended phenolic functions.[42,43]

Considering metal binding, coordination of Cu^{2+}, Zn^{2+}, Cd^{2+}, and Pb^{2+} occurs at acidic pH and leads to full deprotonation of the ligand to afford $[M\mathbf{L^1}(H_{-1})_3]^-$ species (M = Cu^{2+}, Zn^{2+}, Cd^{2+}, and Pb^{2+}). Analysis of the potentiometric data using the HYPERQUAD[40] program does not allow us to determine the constant for the successive ligand deprotonation steps upon metal complexation (*e.g.* the constants for the equilibria $M^{2+} + \mathbf{L^1} = [M\mathbf{L^1}(H_{-1})]^+ + H^+$, $[M\mathbf{L^1}(H_{-1})]^+ = [M\mathbf{L^1}(H_{-1})_2] + H^+$, and $[M\mathbf{L^1}(H_{-1})_2] = [M\mathbf{L^1}(H_{-1})_3]^- + H^+$, M = Cu^{2+}, Zn^{2+}, Cd^{2+}, and Pb^{2+}). This behaviour is probably due to the fact that the three deprotonation steps accompanying metal binding occur in a narrow pH range, *e.g.*, almost simultaneously at very similar pH values. In these cases, the program HYPERQUAD[40] can only calculate the overall constant relative to the simultaneous release of three acidic protons, *e.g.* the constant for the equilibrium $M^{2+} + \mathbf{L^1} = [M\mathbf{L^1}(H_{-1})_3]^- + 3H^+$ (see Table 2). Furthermore, precipitation of the complexes is observed above pH 5–6, precluding the potentiometric study of the systems at neutral and alkaline pH values. However, the data in Table 2 and the distribution diagrams in Fig. 3 show that the Cu^{2+} and Zn^{2+} complexes are remarkably more stable than the corresponding Cd^{2+} and Pb^{2+} ones.

In the case of Cu^{2+} and Zn^{2+}, the binding process occurs at acidic pHs below 3 (Fig. 3a and 3b, for Cu^{2+} and Zn^{2+}, respectively) while the Cd^{2+} and Pb^{2+} complexes start forming around pH 4 (Fig. 3c and 3d, for Cd^{2+} and Pb^{2+}, respectively). This behaviour depends on the greater affinity of the borderline metals Cu^{2+} and Zn^{2+} towards $\mathbf{L^1}$, which contains hard oxygen atoms and borderline N atoms. In the case of the softer cations Cd^{2+} and Pb^{2+} the complexation process occurs at more basic pH values.

The selectivity of $\mathbf{L^1}$ over a set of different metal ions (Cu^{2+}, Zn^{2+}, Cd^{2+}, Pb^{2+}, Al^{3+}, Hg^{2+}, Co^{2+}, Ni^{2+}, Mn^{2+}, Mg^{2+}, K^+, Ca^{2+}, Ag^+, and Na^+) was studied by means of spectrophotometric and spectrofluorimetric titrations in MeCN–H_2O (1 : 1 v/v) buffered at pH 7 with HEPES 1 M (HEPES = 4-(2-hydroxyethyl)-piperazine-1-ethanesulfonic acid). $\mathbf{L^1}$ showed an intense absorption band at 248 nm (ε = 181 100 mol^{-1} cm^{-1} L^{-1}) and a weaker one at 332 nm (ε = 15 900 mol^{-1} cm^{-1} L^{-1}).

Upon addition of increasing amounts of metal ions we observed significant changes in the absorption properties of $\mathbf{L^1}$ in the presence of Cu^{2+}, Zn^{2+}, Cd^{2+}, Pb^{2+}, Hg^{2+}, Co^{2+}, Ni^{2+}, Al^{3+}, and Mn^{2+} (see Fig. 4a for Cd^{2+} and see Fig. S1–S8† for Cu^{2+}, Zn^{2+}, Hg^{2+}, Co^{2+}, Ni^{2+}, Al^{3+}, Mn^{2+} and Pb^{2+}). In particular we observed the disappearance of the bands of the free receptor and the appearance of two new bands at around 260 nm and 390 nm. The formation of three isosbestic points at 254, 282, and 344 nm suggested the presence of only two species in solutions. The absorbance/molar ratio plot (Fig. 4b) at 390 nm

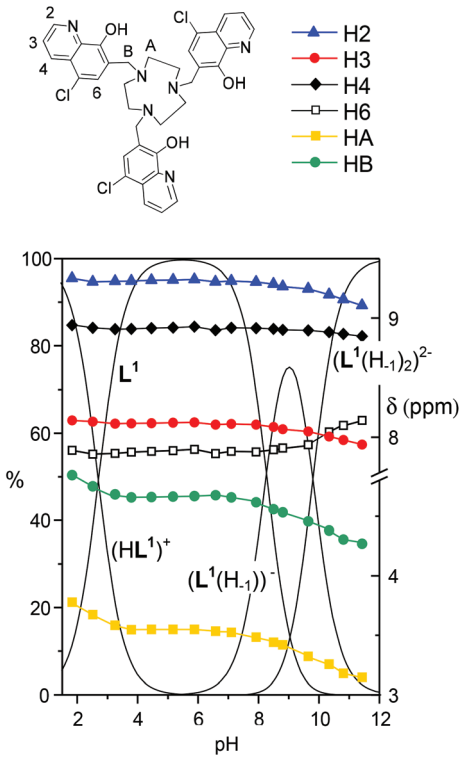

Fig. 2 pH dependence of the ^{1}H-NMR signals of $\mathbf{L^1}$ superimposed on the distribution diagram of the protonated species of $\mathbf{L^1}$ (MeCN–H_2O, 1 : 1 v/v, 298.1 K, 0.10 M NMe_4Cl, [$\mathbf{L^1}$] = 5.0 × 10^{-3} M).

Table 2 Formation constants (log *K*) of the metal complexes with $\mathbf{L^1}$ in MeCN–H_2O (1 : 1 (v/v) at 298.1 K), 0.10 M NMe_4Cl

Reaction	log *K*
$Cu^{2+} + \mathbf{L^1} = [Cu\mathbf{L^1}(H_{-1})_3]^- + 3H^+$	−0.1(1)
$Zn^{2+} + \mathbf{L^1} = [Zn\mathbf{L^1}(H_{-1})_3]^- + 3H^+$	−2.1(1)
$Pb^{2+} + \mathbf{L^1} = [Pb\mathbf{L^1}(H_{-1})_3]^- + 3H^+$	−9.6(1)
$Cd^{2+} + \mathbf{L^1} = [Cd\mathbf{L^1}(H_{-1})_3]^- + 3H^+$	−7.5(1)

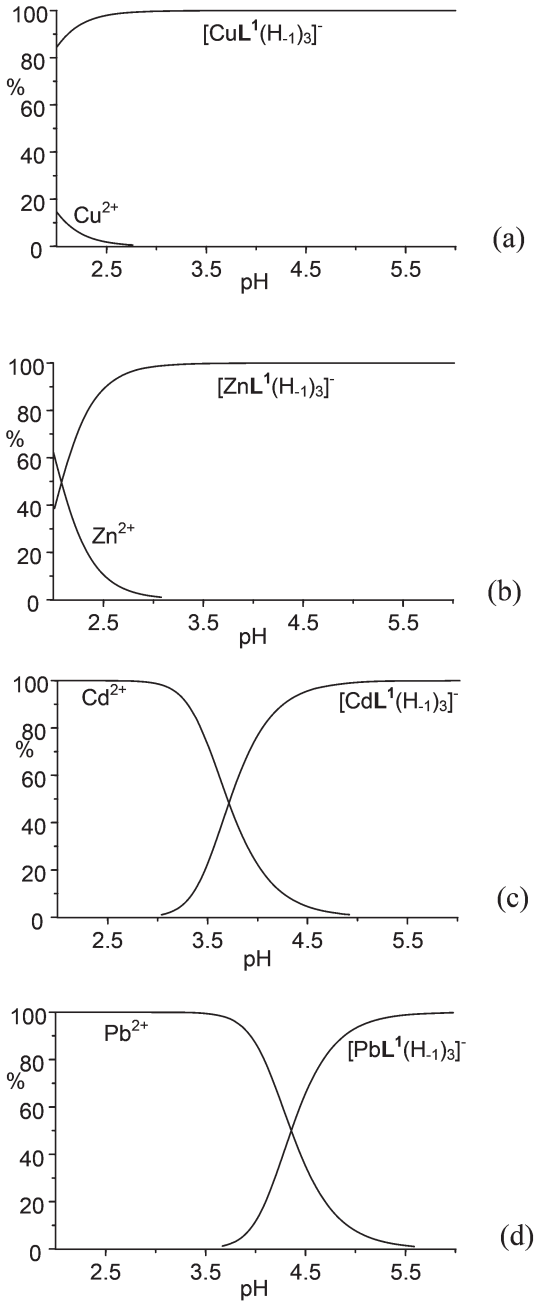

Fig. 3 Distribution diagrams *vs.* pH of the systems $Cu^{2+}/\mathbf{L^1}$ (a), $Zn^{2+}/\mathbf{L^1}$ (b), $Cd^{2+}/\mathbf{L^1}$ (c), and $Pb^{2+}/\mathbf{L^1}$ (d) (MeCN–H_2O, 1 : 1 v/v, 298.1 K, 0.10 M NMe_4Cl, $[\mathbf{L^1}] = 1.0 \times 10^{-3}$ M, $[M^{2+}] = 3.0 \times 10^{-4}$ M).

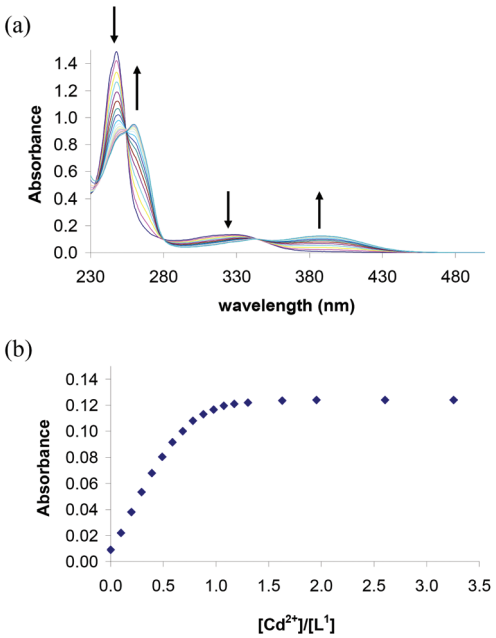

Fig. 4 Changes in the absorption spectra of $\mathbf{L^1}$ ($[\mathbf{L^1}] = 8.0 \times 10^{-6}$ M) (a), and absorbance at 390 nm/molar ratio plot of $\mathbf{L^1}$ upon addition of increasing amounts of Cd^{2+} in MeCN–H_2O 1 : 1 (v/v), pH = 7.0, 298.1 K (b).

suggested the formation of a 1 : 1 metal-to-ligand complex. In the presence of K^+, Mg^{2+}, Ca^{2+}, Ag^+, and Na^+ we did not observe any relevant change in the absorption spectrum of $\mathbf{L^1}$, suggesting that this set of metal ions is not coordinated by the ligand.

The study of the fluorescence properties of $\mathbf{L^1}$ was performed, at first, in a mixture of MeCN–H_2O 1 : 1 (v/v) buffered at pH 7 with HEPES 1 M. In this medium the receptor showed a low intensity emission band at 500 nm when excited at 344 nm ($\Phi = 3.9 \times 10^{-3}$). This low value of fluorescence quantum yields depends on two different mechanisms, namely, intramolecular photoinduced proton transfer (PPT) between the hydroxyl group and the quinoline nitrogen atom and photoinduced electron transfer (PET) between the nitrogen atom of the macrocycle and the 8-HDQ moiety.[44–50] Upon addition of increasing amounts of metal ions (Cu^{2+}, Zn^{2+}, Cd^{2+}, Pb^{2+}, Al^{3+}, Hg^{2+}, Co^{2+}, Ni^{2+}, Mn^{2+}, Mg^{2+}, K^+, Ca^{2+}, Ag^+, and Na^+) we observed a CHEF (chelation enhancement of fluorescence) only in the presence of Cd^{2+} (Fig. 5a) and, to a lesser extent, in the presence of Zn^{2+} and Al^{3+} (see Fig. S9–S11†). Fluorescence intensity/molar ratio plots (Fig. 5b) suggested again the formation of a 1 : 1 metal-to-ligand complex.

For all the other metal ions considered we did not observe any significant change in the emission properties of $\mathbf{L^1}$ (Fig. 6).

Variable pH fluorescence measurements on $\mathbf{L^1}$ and on the system $\mathbf{L^1}/Cd^{2+}$ in MeCN–H_2O (1 : 1 v/v) were compared with the data obtained by potentiometric measurements. In the case of the free ligand (Fig. 7a) both the monoprotonated and the neutral form of $\mathbf{L^1}$ are non-fluorescent. The fluorescence starts increasing with the formation of the $(\mathbf{L^1}(H_{-1}))^-$ species, *e.g.*, with the deprotonation of the chlorohydroxy quinoline moieties. In the case of the $\mathbf{L^1}/Cd^{2+}$ system, Fig. 7b clearly shows that the chemical species responsible for the fluorescence emission is a 1 : 1 complex of $\mathbf{L^1}$ with Cd^{2+}.[51]

In order to assess whether the Cd^{2+}-selective chemosensor is also suitable for biological and environmental applications, we performed some measurements in pure water buffered at pH 7 with HEPES 1 M. Interestingly we observed changes in the UV-Vis properties of $\mathbf{L^1}$ upon addition of increasing amounts of Cd^{2+} (see Fig. S12†); however, the fluorescence of the ligand was not switched ON in this case. This behaviour

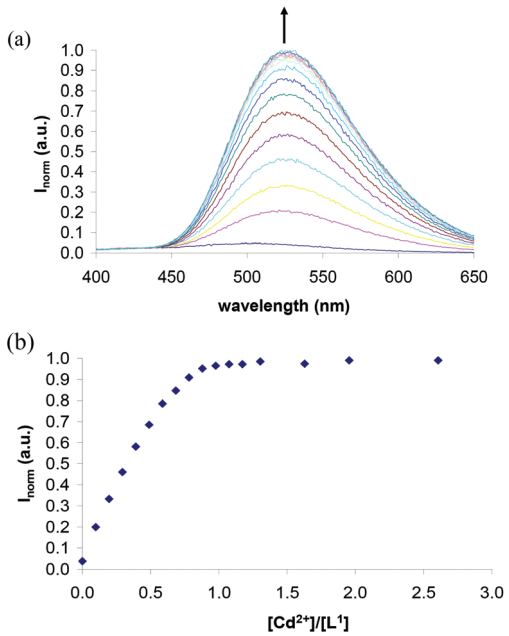

Fig. 5 Changes in the emission spectrum of $\mathbf{L^1}$ ([$\mathbf{L^1}$] = 8.0 × 10^{-6} M, λ_{exc} = 344 nm) (a), and normalised fluorescent intensity/molar ratio plot for $\mathbf{L^1}$ upon addition of increasing amounts of Cd^{2+} in MeCN–H_2O 1 : 1 (v/v), pH = 7.0, 298.1 K, λ_{em} = 530 nm (b).

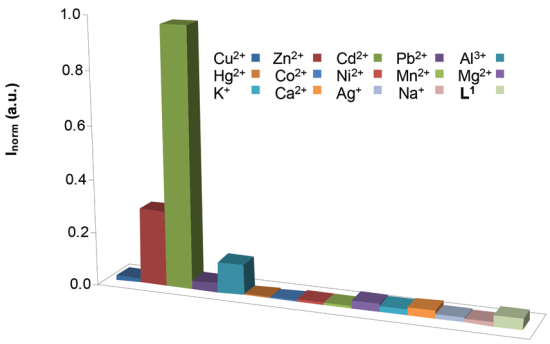

Fig. 6 Effects on the fluorescence intensity of $\mathbf{L^1}$ ([$\mathbf{L^1}$] = 8.0 × 10^{-6} M, λ_{exc} = 344 nm) upon addition of one equivalent of Cu^{2+}, Zn^{2+}, Cd^{2+}, Pb^{2+}, Al^{3+}, Hg^{2+}, Co^{2+}, Ni^{2+}, Mn^{2+}, Mg^{2+}, K^+, Ca^{2+}, Ag^+, and Na^+ in MeCN–H_2O 1 : 1 (v/v).

depends on a further PPT process due to the more polar medium (water instead of a mixture of MeCN–H_2O 1 : 1 (v/v)) that inhibits the radiative decay of the system.

To overcome the lack of a fluorescence response of $\mathbf{L^1}$ to Cd^{2+} in water we decided to encapsulate $\mathbf{L^1}$ in water soluble catanionic-based nanoparticles of a new formulation.

The catanionic system

The structure of the self-assembled aggregates formed in catanionic aqueous mixtures obtained by mixing the double-tailed anionic surfactant NaAOT and the cationic ionic liquid C_{12}mimBr was investigated by means of DLS, SAXS and Cryo-TEM. These catanionic systems were prepared by mixing appropriate amounts of NaAOT and C_{12}mimBr solutions to

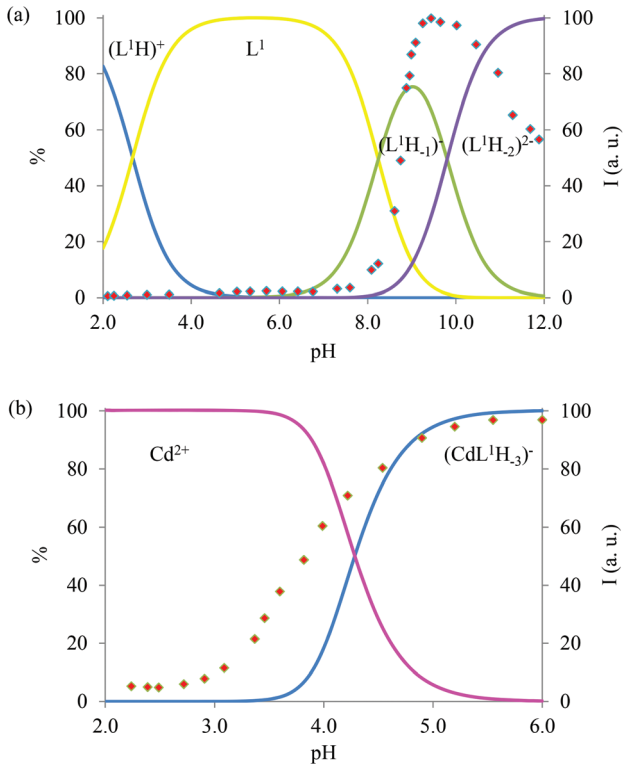

Fig. 7 Distribution diagram *vs.* pH for $\mathbf{L^1}$ ([$\mathbf{L^1}$] = 8.0 × 10^{-6} M (a) and for the $\mathbf{L^1}$/Cd^{2+} system (b) in MeCN–H_2O (1 : 1 v/v) in NH_4Cl 0.1 M, 298.1 K, and (♦) spectrofluorimetric emission intensities at 530 nm at different pH values.

obtain samples with different molar ratios (9 : 1, 8 : 2, 7 : 3, 5 : 5, 2 : 8, 1 : 9). From a macroscopic viewpoint, NaAOT and C_{12}mimBr 22.4 mM aqueous solutions are, respectively, fluid and transparent vesicular or micellar systems. Indeed, in water at a concentration of 18 mM, NaAOT forms vesicles with a mean diameter of 140 nm,[52] while C_{12}mimBr, up to 10.9 mM,[53] forms micelles with an average hydrodynamic radius of 1.4 nm.[54] When the two solutions were mixed together, a series of phase changes were observed when the molar ratio was varied.

Samples belonging to the anionic rich side (NaAOT/C_{12}mimBr molar ratios 9 : 1, 8 : 2, 7 : 3) appear bluish, indicating the formation of a colloidal suspension of nanoparticles of 100 to 200 nm in size.[35] Similarly, samples belonging to the cationic rich side (NaAOT/C_{12}mimBr molar ratios 2 : 8 and 1 : 9) are still bluish, although sample 1 : 9 appeared almost transparent. In contrast, when the two surfactants were mixed in equimolar ratio, the formation of a precipitate in a clear solution was observed. Such a precipitate formation is due to the neutralization of the two opposite charged surfactants' headgroup (AOT^- and $C_{12}mim^+$). This preliminary inspection proved that nanoparticles form in both the anionic and the cationic rich region of the catanionic mixture.

The size and morphology of the self-assembled aggregates were firstly established by means of a Cryo-TEM analysis. This investigation was performed on a selected sample, namely NaAOT/C_{12}mimBr 7 : 3, and the corresponding micrograph is

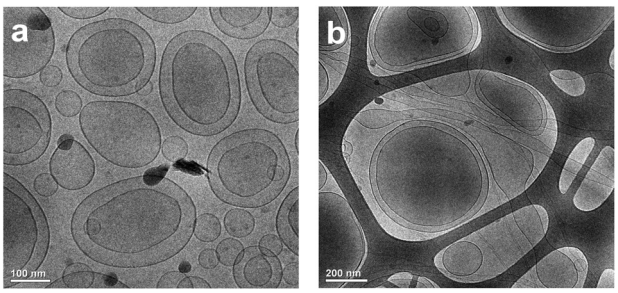

Fig. 8 Cryo-TEM images of the catanionic vesicles obtained by mixing 22.4 mM water solutions of NaAOT and C_{12}mimBr in the molar ratio of 7 : 3.

shown in Fig. 8. The latter evidenced that the catanionic mixture was mainly composed of small single- and double-walled vesicles (Fig. 8a) whose sizes were in good agreement with the bluish appearance of the solutions.[35] At the same time, extremely long (in the range of micrometers) tubular vesicles were also observed (Fig. 8b).

The changes of the vesicles' mean size and ζ-potential as a function of the NaAOT/C_{12}mimBr molar ratios were investigated through DLS measurements. The various NaAOT/C_{12}mimBr mixtures were prepared in a highly dilute regime (0.01 wt%), and experiments were performed at 25 °C. The results, summarized in Table 3, evidenced the formation of aggregates of different sizes and ζ-potentials, depending on the composition of the catanionic mixture.

According to cryo-TEM observations, the vesicle sizes measured in the various catanionic mixtures roughly fall in the 150–200 nm range. Besides, on the basis of the measured ζ-potential values, samples on the NaAOT rich side are endowed with good stability (ζ-potentials < −40 mV), while samples on the C_{12}mimBr rich side possess only a limited stability (ζ-potentials < 10 mV).

The bilayer structure was investigated by SAXS. Measurements were performed on the catanionic mixture with the composition NaAOT/C_{12}mimBr 7 : 3. In this case, due to the scarce signal intensity, samples were prepared in water with a dispersed phase concentration of 3 wt% in order to obtain sufficiently intense scattering curves. It is worth noting that this concentration leads to quite unstable aggregates (around three weeks). The system exhibited a pure diffuse scattering curve (see Fig. S13†), typical of uncorrelated bilayers (*e.g.* small unilamellar vesicles). The bilayer thickness d_B calculated with GAP (see the ESI†) was found to be equal to 35.2 Å in good agreement with the typical dimension of pure AOT bilayers.

Bearing in mind our previous results obtained for a similar receptor (namely 5-(5-chloro-8-hydroxyquinolinyl-7-methyl)-2,8-dithia-5-aza-2,6-pyridinophane) encapsulated in SDS micelles and in liposomes,[14] the bilayer structure of these new catanionic vesicles appeared to be a suitable matrix for the hydrophobic chemosensor **L**^{1} (see ESI† for experimental details) to overcome the lack of fluorescence response in water.

As expected, in this environment we observed an enhancement of the fluorescence emission at 530 nm of **L**^{1} upon excitation at 355 nm in the presence of Cd^{2+}. Although we did not observe a neat plateau, the fluorescence titration data fitted to a 1 : 1 model (log K_{ass} = 4.49(3), Fig. 9). In fact, solutions containing the vesicles were milky opalescent and consequently exhibited high values of scattered light. This allowed us to obtain qualitative information only from absorbance data.

One of the great advantages of the catanionic vesicles compared to micelles or liposomes is that such aggregates exist at very low concentrations. We diluted an aqueous suspension of the vesicles containing the 1 : 1 complex of **L**^{1} with Cd^{2+} up to 400 times (corresponding to a concentration of the complex of 5.3×10^{-8} M) and we were still able to observe a fluorescence response to the presence of Cd^{2+} in water. Unfortunately, the inclusion of **L**^{1} in the catanionic vesicles did not improve the selectivity of the sensor as in the case of the experiments reported in Fig. 6.

Table 3 Mean diameter (D_{AV}), polydispersion index (PDI), and ζ-potential of the various catanionic mixtures

NaAOT : C_{12}mimBr	D_{AV} (nm)	PDI	ζ-Potential (mV)
9 : 1	149 ± 4	0.13	−51 ± 1
8 : 2	162 ± 11	0.16	−43 ± 1
7 : 3	185 ± 9	0.26	−45 ± 1
5 : 5	—	—	—
2 : 8	195 ± 3	0.21	+8.1 ± 0.7
1 : 9	158 ± 6	0.20	+4.2 ± 0.4

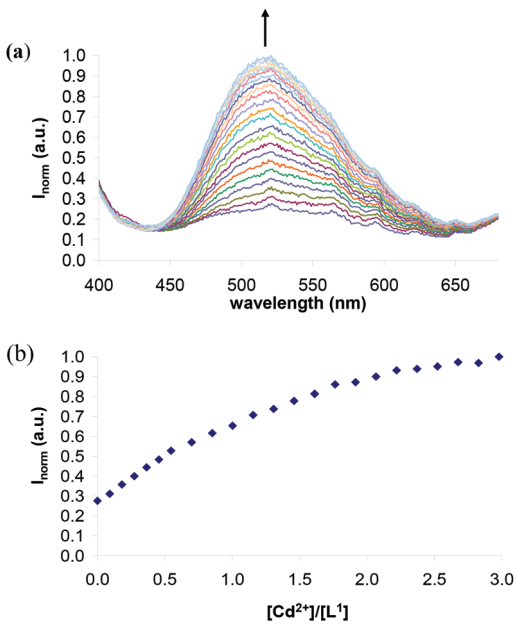

Fig. 9 Changes in the emission spectrum of **L**^{1} ([**L**^{1}] = 2.56×10^{-5} M, H_2O, pH = 7.0, HEPES 1 M, 298.1 K, λ_{exc} = 355 nm) in a suspension of vesicles (a), and normalised fluorescent intensity/molar ratio plot for **L**^{1} upon addition of increasing amounts of Cd^{2+} (b); λ_{em} = 520 nm. NaAOT/C_{12}mimBr molar ratio of 7 : 3 (log K_{ass} = 4.49(3) evaluated using Hypspec).[55] K_{ass} is the association equilibrium constant.

Solid state

Despite many attempts we were able to grow crystals suitable for X-ray diffraction analysis (see ESI† for details) only with $\mathbf{L^1}$ and Cu^{2+}. Upon reaction of $\mathbf{L^1}$ with one equivalent of $Cu(ClO_4)_2{\cdot}2H_2O$ in MeCN followed by a slow diffusion of *n*-hexane in a multilayer solution of MeCN and i-propanol we obtained crystals which seemed suitable for structural analysis.

The asymmetric complex unit is composed of two fully deprotonated molecules of $\mathbf{L^1}$ and four Cu^{2+} ions, two penta-coordinated (Cu(1A) and Cu(1B)) and two hexa-coordinated (Cu(2A) and Cu(2B)) with the same coordination spheres for members of each pair of metal centres (Fig. 10, Tables S1 and S2†). In particular, Cu(1A) and Cu(1B) are coordinated by the three nitrogen atoms of the macrocycle (N(1A), N(4A) and N(7A) for Cu(1A) and N(1B), N(4B) and N(7B) for Cu(1B) with bond distances ranging between 2.001(4) and 2.238(4) Å and by the oxygens of two 5-chloro-8-hydroxyquinoline moieties (O(2A) and O(3A) for Cu(1A) and O(2B) and O(3B) for Cu(1B), distances ranging between 1.952(4) and 1.980(4) Å) bound to the macrocyclic unit. The atoms Cu(2A) and Cu(2B) are merely coordinated by the nitrogens and the oxygen atoms of the 5-chloro-8-hydroxyquinoline moieties without any involvement of the macrocyclic donor atoms. In particular, Cu(2A) is coordinated by the oxygens O(2A) and O(3A) and by the nitrogens N(40A) and N(70A) of the 5-chloro-8-hydroxyquinolines bound to the macrocyclic unit coordinating to Cu(1A) and by the oxygen O(1B) and by the nitrogen N(10B) of one of the 5-chloro-8-hydroxyquinolines bound to the macrocycle coordinating to Cu(1B). The coordination sphere of Cu(2B) is similar. For crystallographic details see Table S2.†

The stoichiometry of the complex in the solid state is clearly different from that observed in solution by potentiometric and spectrophotometric measurements. However, the crystal structure confirms that metal binding occurs upon the full deprotonation of the ligand.

Intracellular fluorescent measurements

Finally, we evaluated the ability of $\mathbf{L^1}$ to bind cadmium within cells *in vivo* by confocal microscopy. Cos-7 cells were chosen because they are widely and successfully used for Cd^{2+} recognition in these kinds of experiments.[7] Control cells incubated without $\mathbf{L^1}$ and cadmium (see ESI†) or incubated with only $\mathbf{L^1}$ showed no fluorescence (Fig. 11A–C). In contrast, cells incubated with 20 μL of Cd^{2+} along with $\mathbf{L^1}$ showed high and diffuse fluorescence (% change in relative fluorescence = 625 ± 58 with respect to the control cells in which % change in relative fluorescence = 100 ± 5, the data are means ± S.E.M. of values from 40 independent wells, $P < 0.001$ *versus* the control (ANOVA and Scheffe's test)) throughout the cytoplasm (Fig. 11D–F). This finding indicates that living cells are permeable to the probe that, in turn, responds specifically to changes in intracellular Cd^{2+} levels.

By further using confocal microscopy, we probed the ability of $\mathbf{L^1}$ to track Cd^{2+} in living cells. We observed that in cells incubated with increasing doses of cadmium(II), the intensity of fluorescence increases correspondingly (see Fig. S14†).

In addition, we tested the toxicity of the probe by a resazurin test. Spectrophotometric measurements of the resazurin reduction revealed that treatment with $\mathbf{L^1}$ did not affect the metabolic activity of the cultured cells compared to control cells (% change in relative metabolic activity of cells exposed for 2 hours to $\mathbf{L^1}$ was 28 ± 6 with respect to the control cells in which % change in relative metabolic activity was 100 ± 4). Data are means ± S.E.M. of values from 12 independent wells, $P < 0.05$ *versus* the control (ANOVA and Scheffe's test).

Conclusions

Here, we have described a new chemosensor for Cd^{2+} recognition ($\mathbf{L^1}$) based on the macrocycle 1,4,7-triazacyclononane functionalized with three 5-chloro-8-hydroxyquinoline moieties. We preliminarily studied the coordination chemistry of this system in solution and in the solid state, and then we tested its application as a fluorescent chemosensor in MeCN–H_2O (1 : 1 v/v) observing a good response to Cd^{2+}. We proposed catanionic vesicles of a new formulation obtained by mixing an ionic liquid (C_{12}mimBr) and a traditional surfactant

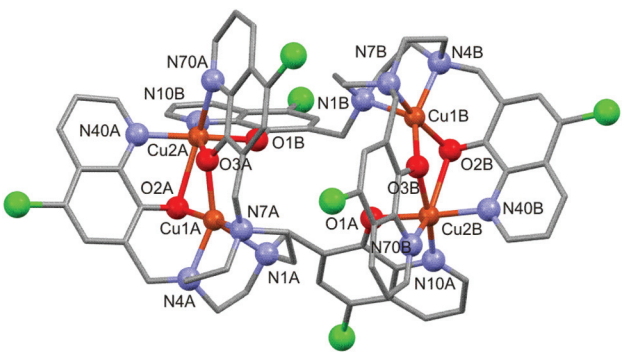

Fig. 10 X-ray crystal structure of the complex ion $[Cu_4(\mathbf{L^1}(H_{-1})_3)_2]^{2+}$ with the adopted numbering scheme. Hydrogens and perchlorate counterions have been omitted for clarity.

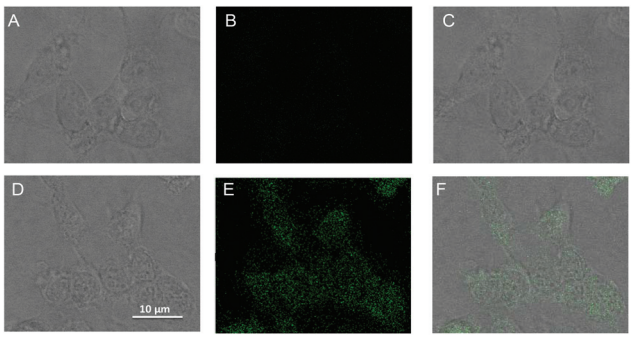

Fig. 11 Confocal visualization of a Cos-7 cell culture in the presence of $\mathbf{L^1}$ (without Cd^{2+}) (A,B,C), and of a Cos-7 cell culture preincubated with 20 μL of Cd^{2+} and in the presence of $\mathbf{L^1}$ (D,E,F). Images were obtained in phase-contrast mode (A,D), in fluorescence mode (B,E), and in merge mode (C,F). Scale bar: 10 μm.

(NaAOT) as a suitable nanocarrier for $\mathbf{L^1}$. In this way we were able to detect Cd^{2+} in water. The development of these novel nanoparticles is promising in overcoming the inconveniences deriving from the scarce solubility and the lack of response in water often presented by organic fluorescent probes. We also demonstrated that $\mathbf{L^1}$ is not cytotoxic and hence it is able to sense Cd^{2+} in living cells, indicating that it is a good candidate for biological applications *in vitro*.

Acknowledgements

Financial support by MIUR (projects PRIN2009-2009Z9ASCA and PRIN 2010BJ23MN_002) and Regione Autonoma della Sardegna (CRP-59699) is gratefully acknowledged. MBH thanks the Leverhulme Foundation for the award of an Emeritus Fellowship. Sardegna Ricerche Scientific Park (Pula, CA, Italy) is acknowledged for free access to facilities of the Nanobiotechnology Laboratory.

Notes and references

1 R. R. Lauwerys, A. M. Bernard and H. A. Reels, *Clin. Chem.*, 1994, **40**, 1391–1394.
2 W. de Vries, P. F. Römkens and G. Schütze, *Rev. Environ. Contam. Toxicol.*, 2007, **191**, 91–130.
3 H. N. Kim, W. X. Ren, J. S. Kim and J. Yoon, *Chem. Soc. Rev.*, 2012, 3210–3244 and references therein.
4 A. C. Davis, C. P. Calloway Jr. and B. T. Jones, *Talanta*, 2007, **71**, 1144–1149.
5 A. N. Anthemidis and C. P. Karapatouchas, *Microchim. Acta*, 2008, **160**, 455–460.
6 A. T. Townsend, K. A. Miller, S. McLean and S. Aldous, *J. Anal. At. Spectrom.*, 1998, **13**, 1213–1219.
7 G. Kaya and M. Yaman, *Talanta*, 2008, **75**, 1127–1133.
8 V. Iyengar and J. Wolttlez, *Clin. Chem.*, 1988, 474–481.
9 A. E. Hargrove, S. Nieto, T. Zhang, J. L. Sessler and E. V. Anslyn, *Chem. Rev.*, 2011, **111**, 6603–6782.
10 D. T. Quang and J. S. Kim, *Chem. Rev.*, 2010, **110**, 6280–6301.
11 J. F. Zhang, Y. Zhou, J. Yoon and J. S. Kim, *Chem. Soc. Rev.*, 2011, **40**, 3416–3429.
12 X. Chen, Y. Zhou, X. Peng and J. Yoon, *Chem. Soc. Rev.*, 2010, **39**, 2120–2135.
13 Y. Zhou, Z. Xu and J. Yoon, *Chem. Soc. Rev.*, 2011, **40**, 2222–2235.
14 M. Mameli, M. C. Aragoni, M. Arca, C. Caltagirone, F. Demartin, G. Farruggia, G. De Filippo, F. A. Devillanova, A. Garau, F. Isaia, V. Lippolis, S. Murgia, L. Prodi, A. Pintus and N. Zaccheroni, *Chem.–Eur. J.*, 2010, **16**, 919–930.
15 M. Taki, M. Desaki, A. Ojida, S. Iyoshi, T. Hirayama, I. Hamachi and Y. Yamamoto, *J. Am. Chem. Soc.*, 2008, **130**, 12564–12565.
16 T. Cheng, Y. Xu, S. Zhang, W. Zhu, X. Qian and L. Duan, *J. Am. Chem. Soc.*, 2008, **130**, 16160–16161.
17 X. Peng, J. Du, J. Fan, J. Wang, Y. Wu, J. Zhao, S. Sun and T. Xu, *J. Am. Chem. Soc.*, 2007, **129**, 1500–1501.
18 S. Banerjee, S. Kar and S. Santra, *Chem. Commun.*, 2008, 3037–3039.
19 H. Li, Y. Yao, C. Han and J. Zhan, *Chem. Commun.*, 2009, 4812–4814.
20 S. A. El-Safty, D. Prabhakaran, A. A. Ismail, H. Matsunaga and F. Mizukami, *Adv. Funct. Mater.*, 2007, **17**, 3731–3745.
21 T. Balaji, S. A. El-Safty, H. Matsunaga, T. Hanaoka and F. Mizukami, *Angew. Chem., Int. Ed.*, 2006, **45**, 7202–7208.
22 Y. Xu, L. Zhao, H. Bai, W. Hong, C. Li and G. Shi, *J. Am. Chem. Soc.*, 2009, **131**, 13490–13497.
23 R. Angelico, M. Carboni, S. Lampis, J. Schmidt, Y. Talmon, M. Monduzzi and S. Murgia, *Soft Matter*, 2013, **9**, 921–928.
24 M. Carboni, A. M. Falchi, S. Lampis, C. Sinico, M. L. Manca, J. Schmidt, Y. Talmon, S. Murgia and M. Monduzzi, *Adv. Healthcare Mater.*, 2013, **2**, 692–701.
25 F. Cuomo, M. Mosca, S. Murgia, A. Ceglie and F. Lopez, *Colloids Surf., B*, 2013, **104**, 239–244.
26 A. Cardone, F. Lopez, F. Affortunato, G. Busco, A. M. Hofer, R. Mallamaci, C. Martinelli, M. Colella and G. M. Farinola, *Biochim. Biophys. Acta*, 2012, **1818**, 2808–2817.
27 R. Angelico, A. Ceglie, G. Colafemmina, F. Lopez, S. Murgia, U. Olsson and G. Palazzo, *Langmuir*, 2005, **21**, 140–148.
28 P. Hiwale, S. Lampis, G. Conti, C. Caddeo, S. Murgia, A. M. Fadda and M. Monduzzi, *Biomacromolecules*, 2011, **12**, 3186–3193.
29 S. Murgia, P. Fadda, G. Colafemmina, R. Angelico, L. Corrado, P. Lazzari, M. Monduzzi and G. Palazzo, *J. Colloid Interface Sci.*, 2013, **390**, 129–136.
30 B. Sivakumar, R. G. Aswathy, Y. Nagaoka, M. Suzuki, T. Fukuda, Y. Yoshida, T. Maekawa and D. N. Sakthikumar, *Langmuir*, 2013, **29**, 3453–3466.
31 F. Cuomo, F. Lopez, L. Maiuro, A. Ceglie, M. G. Miguel and B. Lindman, *Soft Matter*, 2012, **8**, 4415–4420.
32 J. Bhattacharjee, V. K. Aswal, P. A. Hassan, R. Pamu, J. Narayanan and J. Bellare, *Soft Matter*, 2012, **8**, 10130–10140.
33 R. O. Brito, E. F. Marques, S. G. Silva, M. L. do Vale, P. Gomes, M. J. Araújo, J. E. Rodriguez-Borges, M. R. Infante, M. T. Garcia and I. Ribosa, *Colloids Surf., B*, 2009, **72**, 80–87.
34 Y. Jiang, F. Li, Y. Luan, W. Cao, L. Zhao, L. Zhang and Z. Li, *Int. J. Pharm.*, 2012, **436**, 806–814.
35 E. F. Marques, *Langmuir*, 2000, **16**, 4798–4807.
36 S. Murgia, M. Monduzzi, F. Lopez and G. Palazzo, *J. Solution Chem.*, 2013, **42**, 1111–1122.
37 S. Murgia, G. Palazzo, M. Mamusa, S. Lampis and M. Monduzzi, *J. Phys. Chem. B*, 2009, **113**, 9216–9225.
38 T. J. Atkins, *J. Am. Chem. Soc.*, 1980, **102**, 6364–6365.
39 G. Ambrosi, M. Formica, V. Fusi, L. Giorgi and M. Micheloni, *Coord. Chem. Rev.*, 2008, **252**, 1121–1152.
40 P. Gans, A. Sabatini and A. Vacca, *Talanta*, 1996, **43**, 1739–1753.
41 H. Steger and A. Corsini, *J. Inorg. Nucl. Chem.*, 1973, **35**, 1621–1636.

42 A. Bencini, C. Coluccini, A. Garau, C. Giorgi, V. Lippolis, L. Messori, D. Pasini and S. Puccioni, *Chem. Commun.*, 2012, **48**, 10428–10430.
43 E. Arturoni, C. Bazzicalupi, A. Bencini, C. Caltagirone, A. Danesi, A. Garau, C. Giorgi, V. Lippolis and B. Valtancoli, *Inorg. Chem.*, 2008, **47**, 6551–6563.
44 E. Bardez, I. Devol, B. Larrey and B. Valeur, *J. Phys. Chem. B*, 1997, **101**, 7786–7793.
45 L. Prodi, C. Bargossi, M. Montalti, N. Zaccheroni, N. Su, J. S. Bradshaw, R. M. Izatt and P. B. Savage, *J. Am. Chem. Soc.*, 2000, **122**, 6769–6770.
46 L. Prodi, M. Montalti, J. S. Bradshaw, R. M. Izatt and P. B. Savage, *J. Inclusion Phenom. Macrocyclic Chem.*, 2001, **41**, 123–127.
47 M. Goldman and E. L. Wehry, *Anal. Chem.*, 1970, **42**, 1178–1185.
48 M. R. Nimlos, D. F. Kelley and E. R. Bernstein, *J. Phys. Chem.*, 1987, **91**, 6610–6614.
49 R. T. Bronson, M. Montalti, L. Prodi, N. Zaccheroni, R. D. Lamb, N. K. Dalley, R. M. Izatt, J. S. Bradshaw and P. B. Savage, *Tetrahedron Lett.*, 2004, **45**, 11139–11144.
50 S. G. Schulman, *Anal. Chem.*, 1971, **43**, 285–287.
51 The discrepancy observed between the distribution diagram and the spectrofluorimetric intensity could be attributed to the different experimental conditions.
52 R. Saha, P. K. Verma, R. K. Mitra and S. K. Pal, *Colloids Surf., B*, 2011, **88**, 345–353.
53 B. Dong, N. Li, L. Zheng, L. Yu and T. Inoue, *Langmuir*, 2007, **23**, 4178–4182.
54 Y. Gu, L. Shi, X. Cheng, F. Lu and L. Zheng, *Langmuir*, 2013, **29**, 6213–6220.
55 P. Gans, *HypSpec*, Protonic Software, Leeds, 2006.